The Nano-scale Barrier Layer Engineering in Addressing Sodium Ion-Related Degradation in SHJ Cells

Xinyuan Wu[1], Chandany Sen[1], Haoran Wang[1], Xutao Wang[1], Yutong Wu[2], Muhammad Umair Khan[1], Lizhong Mao[2], Fangdan Jiang[2], Tao Xu[2], Guangchun Zhang[2], and Bram Hoex[1,*]

[1] School of Photovoltaic and Renewable Energy Engineering, University of New South Wales, Sydney, Australia
[2] Canadian Solar Inc., Suzhou, China
b.hoex@unsw.edu.au

Silicon heterojunction (SHJ) solar cells are well-known for their exceptional efficiency. SHJ solar cells have reached an outstanding level of power conversion efficiency (PCE) performance, with Longi establishing a groundbreaking global record of 26.81% in 2022 [1,2]. This remarkable achievement demonstrates the significant progress made in SHJ technology, propelling the advancement of solar energy utilization to new heights. However, they are vulnerable to various contaminants, resulting in significant performance decline when exposed to damp-heat conditions like DH85 (85°C and 85% relative humidity). Ensuring the long-term stability of silicon photovoltaic (PV) modules is crucial to extend their lifespan [3,4]. One of the factors responsible for degradation in silicon solar modules under damp-heat conditions is the presence of sodium ions (Na^+) [5,6]. This study focuses on investigating the impact of an ultra-thin AlO_x capping layer (approximately 10 nm thick) in preventing the failure of SHJ cells caused by Na^+-related contaminants after DH85 testing. The research reveals that SHJ cells experience a significant relative power drop of around 30% after only 20 hours of DH85 testing. This deterioration affects both the front and rear sides of the cells, primarily due to the silver contact's degradation, leading to increased series resistance and recombination, resulting in a significant decrease in open-circuit voltage (V_{oc}), particularly on the rear side. However, the application of an AlO_x barrier layer to the SHJ cells substantially reduces the performance losses caused by Na^+-related contaminants to approximately 3.3%$_{rel}$. The loss in V_{oc} on the rear side is completely suppressed, and there is only a slight increase of about 50%$_{rel}$ in series resistance (R_s), as opposed to the approximately 300%$_{rel}$ increase observed in cells without the AlO_x barrier layer. These findings demonstrate that the ultra-thin AlO_x barrier layer effectively shields SHJ cells from Na^+, mitigating both R_s and recombination losses. Moreover, the AlO_x barrier layer deposition method is compatible with existing industrial mass-production ALD tools, presenting a viable cell-level solution for SHJ cells. This approach holds promise for enhancing the overall performance and durability of SHJ solar cells.

Experiments

For the experiments, all the samples utilized were M10 half-cut n-type industrial silicon SHJ cells (182 mm×91 mm) with 10 busbars. The structure is shown as Figure 1 (a). The samples were then divided into three categories: 1) Control group with no barrier layer and no exposure to Na^+ contaminant, 2) Group with no barrier layer but exposed to Na+ contaminants, and 3) Group with a barrier layer and exposed to Na+ contaminants. In Group 3, an around 10 nm AlO_x barrier layer was deposited onto the entire SHJ cells, as depicted in Figure 1(a). The deposition of AlO_x layers was performed using an industrial batch ALD reactor (Leadmicro QL200). The metal precursor used was trimethylaluminum (TMA), while deionized water (DIW) served as the oxidant. Subsequently, all samples from both Group 2 and Group 3 underwent exposure to a 0.9 wt.% sodium chloride (NaCl) solution, which served as the source of Na^+ contaminants for the experiment. The experimental procedure is outlined in Figure 1(b). About 0.2 g of NaCl solution was evenly sprayed onto the test surface of each sample, and then they were naturally dried in a fume cupboard. Following this, the control samples (Group 1) and the contaminated samples (Groups 2 and 3) were placed inside an ASLi Environment chamber, where the temperature was maintained at 85°C, with a relative humidity of 85%. The climate chamber was periodically cooled to room temperature to facilitate the characterization of the samples.The current-voltage (I-V) characteristics of the samples were measured using a LOANA solar cell analysis system from PV tools. Photoluminescence (PL) and

series resistance (R_s) images were captured using a BTimaging R3 tool equipped with a high open-circuit voltage lens. Luminescence images were further processed using LumiTools [7]. The contact resistivity (ρ_c) was measured through the transfer length method (TLM) with customized samples employing a PV-tools TLM-SCAN$^+$. Scanning electron microscopy (SEM) images were obtained using the FEI Nova NanoSEM 450 FE-SEM at 10 kV, with a working distance of approximately 5 mm. For energy dispersive spectroscopy (EDS), the Oxford Instruments Ultim® Max detector was used, and the results were analyzed using AZtec software.

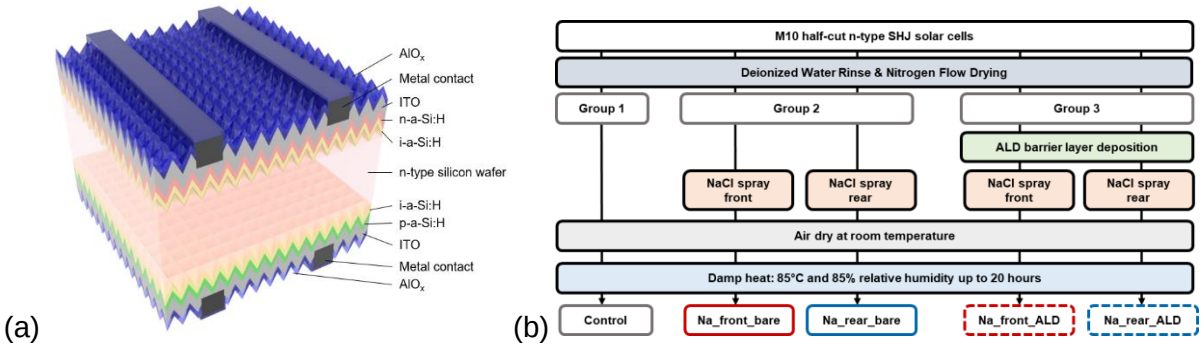

Figure 1. (a) Schematic of SHJ solar cells with an AlO_x barrier layer (not to scale) and (b) experiment flow chart.

Results and discussion

Table 1 The average cell performance comparison before and after the ALD process.

	PCE (%)	J_{sc} (mA/cm^2)	V_{oc} (mV)	FF (%)
Before ALD process	24.0	39.3	741.9	82.3
After ALD process	24.0	39.2	741.9	82.6

Table 1 displays the alterations in I-V parameters observed before and after the ALD AlO_x barrier layer deposition Notably, no substantial changes were detected in any of the parameters following the application of the ALD AlO_x barrier layer. The measured power conversion efficiency (PCE) of the cells remained at approximately 24%. And the main parameter change of the cells can be neglected.

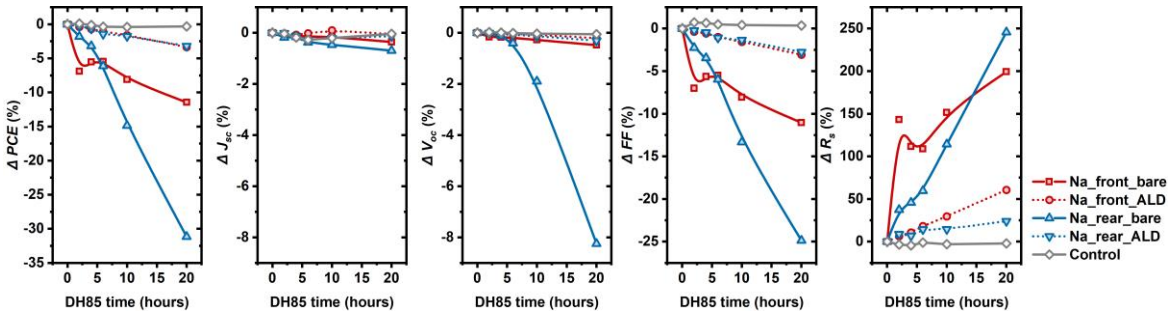

Figure 2. Relative changes in PCE, J_{sc}, V_{oc}, FF and R_s as a function of DH85 duration for the various sample groups shown in Figure 1.

In the 20-hour DH85 test, the control group exhibited only minor power conversion efficiency (PCE) attenuation, and key parameters such as short-circuit current (J_{sc}), V_{oc}, fill factor (FF), and R_s remained relatively stable, as depicted in Figure 2. These results indicate that moisture alone, during the 20-hour DH85 test duration in this study, did not lead to significant losses in SHJ cells. However, the Na_front_bare and Na_rear_bare samples displayed pronounced PCE degradation (~11.4%$_{rel}$ and ~33.5%$_{rel}$, respectively) after the 20-hour DH85 test. For the Na_front_bare samples, R_s increased by up to 143%$_{rel}$ in the first two hours, resulting in a decrease in FF from 82.5% to 76.9%. Nevertheless, no substantial changes in J_{sc} and V_{oc} were observed in the Na_front_bare samples.

On the other hand, for the Na_rear_bare samples, R_s increased linearly with time and was significantly higher than in Na_front_bare samples. Moreover, the V_{oc} of Na_rear_bare samples began to decrease after 6 hours, with a loss of ~8.2%$_{rel}$ after 20 hours of DH85 testing. Conversely, the samples with AlO_x barrier layer, Na_front_ALD and Na_rear_ALD, exhibited only a minor drop in PCE after 20 hours of DH85 testing. This drop in PCE was also attributed to an increase in R_s, but the extent of loss was significantly less than in the Na_front_bare and Na_rear_bare samples. Furthermore, the increase in R_s for the AlO_x barrier layer samples was less severe compared to the samples without the AlO_x barrier layer. Notably, no significant loss of V_{oc} was observed in the Na_rear_ALD samples.

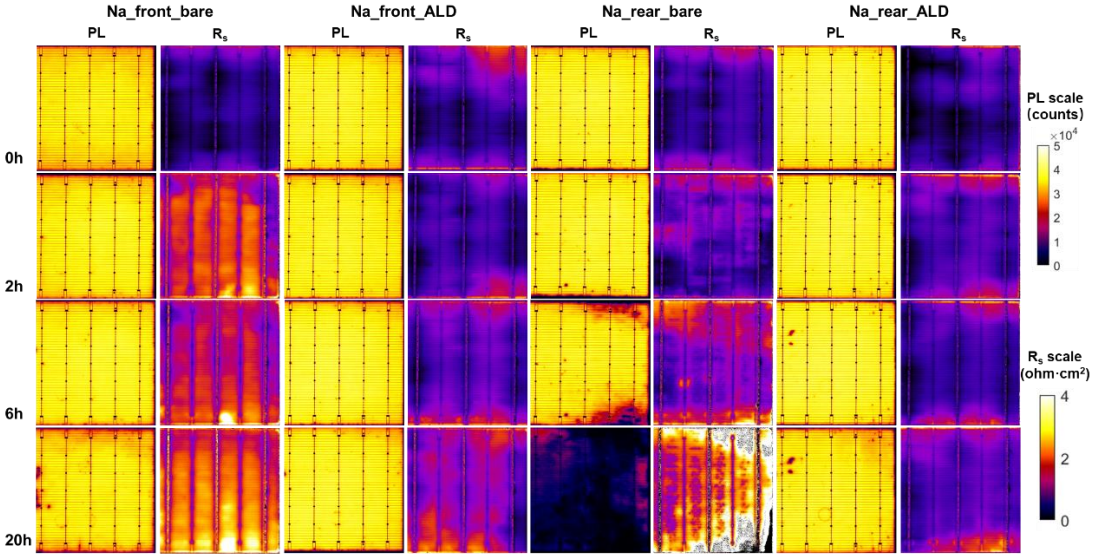

Figure 3 PL and R_s images of SHJ solar cells from four experimental groups during the NaCl-induced DH85 test (0, 2, 6 and 20 h). See Figure 1 for a description of the samples.

As shown in Figure 3, for the Na_front_bare cells, no significant variations in PL intensities were observed throughout the test process, indicating no recombination losses in these samples. However, there was a rapid increase in R_s within the first two hours, mainly concentrated in the finger regions between busbars. The failure in R_s remained localized between the busbars but gradually expanded as the DH85 test continued. As for the Na_rear_bare cells, a significant decline in PL intensity was observed after the DH85 test. This decline originated at the cell's edge after six hours and gradually spread throughout the entire cell area. The variation trend in R_s for Na_rear_bare cells differed from that of Na_front_bare cells. In the initial 2 hours, only a slight non-uniform increase in R_s was observed between the busbars. However, after 6 hours of the DH85 test, the R_s at the edge area of the cells began to increase, becoming more noticeable after 20 hours. In contrast, cells with an AlO_x barrier layer and pre-exposed to NaCl on either the front or rear side (Na_front_ALD and Na_rear_ALD) exhibited minimal to no significant changes in PL intensities even after 20 hours of the DH85 test. These cells also showed no noticeable degradation at the edges, indicating the effectiveness of the AlO_x barrier layer in preventing recombination loss caused by Na^+ penetration. After the first 6 hours of the DH85 test, the increase in R_s could be neglected. These observations align with the earlier discussed I-V results, which indicated a significant decrease in V_{oc}, particularly in Na_rear_bare cells and to a lesser extent in Na_front_bare cells, while Na_front_ALD and Na_rear_ALD cells remained unaffected.

In the study, we conducted EDS analysis on the samples and discerned a notable concurrence between the front and rear sides. Consequently, Figure 5 is exclusively dedicated to presenting the succinctly summarized findings concerning the outcomes of front-side metal contacts subsequent to a 20-hour DH85 test. This visualization effectively highlights the shielding attributes of the AlO_x barrier layer. The “TruMap” algorithm was applied to correct the EDS images and censure that the algorithm efficiently eliminates background noise and deconvolutes X-ray peaks[8]. Figure 5 (a)

showcases the presence of Na and Cl on the surface, with consistently robust signals of Na and Cl evident in the images. After “TruMap” processing, the lighter regions might signify the penetration of Na and Cl into the substrate. On the other hand, Figure 5 (b) pertains to Na_front_ALD, revealing a uniformly strong Na signal across both the metal and ITO regions.

However, a comparative analysis between Figure 5 (a) and (b) reveals dissimilarity between Cl signals and Na signals in Na_front_ALD. This discrepancy implies that the AlOx layer effectively separated the combination of Na and Cl, allowing sodium to persist on the cell's surface. This preservation of sodium on the surface, in turn, facilitated the effective mitigation of metal failure induced by NaCl solution, as evidenced by the discrepancy in Ag signals. Moreover, the protective effects of the AlOx layer proved advantageous in reducing recombination losses, particularly at the rear side of the cell.

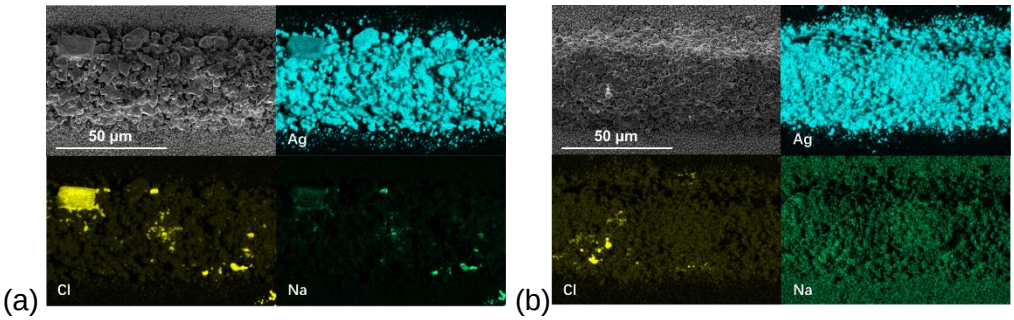

Figure 5. Top-view SEM and EDS images of (a) Na_front_bare and (b) Na_front_ALD samples. See Figure 1 for a description of the samples.

Conclusion

In conclusion, we revealed a Na^+-related degradation mode of SHJ solar cells under DH85. The relative power conversion efficiency loss could be up to ~33.5%, mainly caused by R_s and V_{oc} failures. According to a series of characterizations, corresponding evidence pointed out that this degradation mainly occurred in the metal contact due to the collective effect of Na^+ and Cl^- under DH85. In addition, this work expresses a feasible, compatible, and operable method for enhancing the stability of SHJ solar cells. We used an industrial batch-type thermal ALD system to deposit an ALD AlO_x barrier layer on SHJ solar cells without additional performance loss. This ALD AlO_x barrier layer effectively maintained the SHJ cells' performance under NaCl-induced degradation. The analysis showed that the capping AlO_x layer mainly obstructed the Na^+ penetration and protected the industrial SHJ cells.

References

1 Green, M. A. *et al.* Solar cell efficiency tables (Version 61). *Progress in Photovoltaics: Research and Applications* **31**, 3-16 (2023). https://doi.org/10.1002/pip.3646

2 Lin, H. *et al.* Silicon heterojunction solar cells with up to 26.81% efficiency achieved by electrically optimized nanocrystalline-silicon hole contact layers. *Nature Energy* (2023). https://doi.org/10.1038/s41560-023-01255-2

3 Peters, I. M., Hauch, J., Brabec, C. & Sinha, P. The value of stability in photovoltaics. *Joule* **5**, 3137-3153 (2021). https://doi.org/https://doi.org/10.1016/j.joule.2021.10.019

4 Arriaga Arruti, O., Virtuani, A. & Ballif, C. Long-term performance and reliability of silicon heterojunction solar modules. *Progress in Photovoltaics: Research and Applications* (2023). https://doi.org/10.1002/pip.3688

5 Li, X. *et al.* Potential-free sodium-induced degradation of silicon heterojunction solar cells. *Progress in Photovoltaics: Research and Applications* (2023). https://doi.org/10.1002/pip.3698

6 Adachi, D., Terashita, T., Uto, T., Hernández, J. L. & Yamamoto, K. Effects of SiOx barrier layer prepared by plasma-enhanced chemical vapor deposition on improvement of long-term reliability and production cost for Cu-plated amorphous Si/crystalline Si heterojunction solar cells. *Solar Energy Materials and Solar Cells* **163**, 204-209 (2017). https://doi.org/https://doi.org/10.1016/j.solmat.2016.12.029

7 Payne, D. N. R., Vargas, C., Hameiri, Z., Wenham, S. R. & Bagnall, D. M. An advanced software suite for the processing and analysis of silicon luminescence images. *Computer Physics Communications* **215**, 223-234 (2017). https://doi.org/https://doi.org/10.1016/j.cpc.2017.02.012

8 Burgess, S. *et al.* Five Years of Live Chemical Imaging: From the First Live Maps to Real-time Dynamic Imaging Combining Morphology and Chemistry with Overlap Corrected EDS Data. *Microscopy and Microanalysis* **28**, 516-517 (2022). https://doi.org/10.1017/s1431927622002690